4080–4092 *Nucleic Acids Research, 2013, Vol. 41, No. 7* *Published online 28 February 2013*
doi:10.1093/nar/gkt134

The PARP3- and ATM-dependent phosphorylation of APLF facilitates DNA double-strand break repair

Amanda L. Fenton[1,2], Purnata Shirodkar[1,2], Chloe J. Macrae[1,2], Li Meng[1] and C. Anne Koch[1,2,3,*]

[1]Division of Signalling Biology, Ontario Cancer Institute (University Health Network), 610 University Avenue, Toronto, Ontario M5G 2M9, Canada, [2]Department of Medical Biophysics, University of Toronto, 25 King's College Circle Toronto, Ontario M5S 1A1, Canada and [3]Radiation Medicine Program, Princess Margaret Hospital (University Health Network), 610 University Avenue, Toronto, Ontario M5G 2M9, Canada

Received November 18, 2012; Revised January 23, 2013; Accepted February 10, 2013

ABSTRACT

APLF is a forkhead associated-containing protein with poly(ADP-ribose)-binding zinc finger (PBZ) domains, which undergoes ionizing radiation (IR)-induced and Ataxia-Telangiectasia Mutated (ATM)-dependent phosphorylation at serine-116 (Ser^{116}). Here, we demonstrate that the phosphorylation of APLF at Ser^{116} in human U2OS cells by ATM is dependent on poly(ADP-ribose) polymerase 3 (PARP3) levels and the APLF PBZ domains. The interaction of APLF at sites of DNA damage was diminished by the single substitution of APLF Ser^{116} to alanine, and the cellular depletion or chemical inhibition of ATM or PARP3 also altered the level of accumulation of APLF at sites of laser-induced DNA damage and impaired the accumulation of Ser^{116}-phosphorylated APLF at IR-induced γH2AX foci in human cells. The data further suggest that ATM and PARP3 participate in a common signalling pathway to facilitate APLF-Ser^{116} phosphorylation, which, in turn, appears to be required for efficient DNA double-strand break repair kinetics and cell survival following IR. Collectively, these findings provide a more detailed understanding of the molecular pathway that leads to the phosphorylation of APLF following DNA damage and suggest that Ser^{116}-APLF phosphorylation facilitates APLF-dependent double-strand break repair.

INTRODUCTION

DNA damage leads to the orchestration of a coordinated cascade of events, known as the DNA damage response (DDR), which is important for the maintenance of genomic integrity and the prevention of large-scale genomic aberrations, which can lead to cell death and cancer (1–4). Following detection of the DNA lesion, cells coordinate the activation of cell cycle checkpoints and DNA repair (1–4). An important aspect of the DDR is the recruitment of proteins to the lesion in an organized manner, which is regulated in part by post-translational modifications, including protein phosphorylation and poly(ADP-ribosyl)ation (5).

One of the major protein kinases mediating protein phosphorylation at the sites of DNA damage is Ataxia-Telangiectasia Mutated (ATM), which belongs to the phosphoinositide-3-kinase-related serine/threonine protein kinase (PIKK) family, which also includes Ataxia-Telangiectasia and Rad3 (ATR) related and DNA-dependent protein kinase, catalytic subunit (DNA-PKcs) (6–8). Unlike ATR activity, which is associated with single-strand DNA breaks (SSBs), the activation of ATM and DNA-PKcs occurs mainly in response to DNA double-strand breaks (DSBs) (6). Notably, phosphorylation by ATM of downstream targets is known to regulate not only the activity of the proteins in the DDR but also facilitates the association of the DDR proteins with chromatin following damage (9,10).

Another critical post-translational modification associated with the DDR is the synthesis of poly(ADP-ribose) (PAR) by poly(ADP-ribose) polymerases (PARPs) (11,12). Human PARPs constitute a large family of mammalian proteins that synthesize and transfer ADP-ribose polymers onto glutamate, aspartate or lysine residues of acceptor proteins (13). Of these, PARP1 and PARP2 are the best-studied members of the PARP family, and their catalytic activity is induced in the presence of DNA lesions, mainly SSBs, playing a key role in maintenance of genome integrity (14).

Recently, PARP3, which is highly related to PARP1 and PARP2, has been shown to be activated specifically by DSBs *in vitro* (15). Unlike PARP1, PARP3 does not

*To whom correspondence should be addressed. Tel: +1 416 946 4662; Fax: +1 416 946 2111; Email: anne.koch@rmp.uhn.on.ca

© The Author(s) 2013. Published by Oxford University Press.
This is an Open Access article distributed under the terms of the Creative Commons Attribution Non-Commercial License (http://creativecommons.org/licenses/by-nc/3.0/), which permits unrestricted non-commercial use, distribution, and reproduction in any medium, provided the original work is properly cited.

contain a DNA-binding domain composed of zinc fingers. Despite this, PARP3 has been shown to interact with chromatin and to bind to DNA *in vitro* (15,16). Furthermore, knockdown of PARP3, but not PARP1 or PARP2, has been reported to cause a significant delay in the repair of ionizing radiation (IR)-induced γH2AX foci and leads to an increase in the production of IR-induced DSBs (17). In keeping with a role in DSB repair, PARP3 interacts with the DNA repair factor APLF [aprataxin polynucleotide kinase phosphatase (PNKP)-like factor] and appears to accelerate the accumulation of APLF at DSBs (15). Furthermore, APLF promotes the association of the XRCC4/ligase IV end-joining complex in chromatin (15). Collectively, these data are consistent with a role for PARP3 and APLF in non-homologous end-joining (NHEJ).

Central to the DDR is the recruitment and accumulation of proteins involved in the timely repair of DNA lesions. APLF participates in the DDR and contains a forkhead-associated (FHA) domain, tandem PAR-binding zinc finger (PBZ) domains, a conserved acidic motif possessing homology to the NAP1L family of histone chaperones, and undergoes ATM-dependent phosphorylation following DNA damage (18–21). The FHA domain mediates phosphothreonine-dependent interactions with the DNA repair proteins XRCC1 and XRCC4, whereas the tandem PBZ domains facilitate the initial recruitment of APLF to DNA damage, in a PAR-dependent manner (18,20). APLF also interacts with the Ku heterodimer, participates in DSB repair and is required for the cellular resistance to a variety of DNA damaging agents (18,22).

Although several reports have contributed to our understanding of the APLF FHA and PBZ domains, the functional consequence(s) of APLF phosphorylation by ATM is not known but is consistent with a role for APLF in the DDR. Herein, we show that the tandem PBZ domains and PARP3 are required for the ATM-dependent phosphorylation of APLF at Ser^{116}. Furthermore, we establish that APLF-Ser^{116} phosphorylation contributes to the association of APLF with chromatin and promotes DSB repair and cell survival following DNA damage.

MATERIALS AND METHODS

Cloning and plasmid constructions

The cloning of pcDNA3.1/V5-APLF, pcDNA3.1/V5-$APLF^{S116A}$, wild-type (WT) pEGFPC2-APLF, pEGFPC2-$APLF^{PBZ1m}$, pEGFPC2-$APLF^{PBZ2m}$ and pEGFPC2-$APLF^{Y381A}$ has been described previously (18,20). Quikchange site-directed mutagenesis (Stratagene) was used to create the plasmids pcDNA3.1/V5-$APLF^{S116D}$ using pcDNA3.1/V5-APLF, and pEGFPC2-$APLF^{S116A}$ and pEGFPC2-$APLF^{S116D}$ using pEGFPC2-$APLF^{WT}$ as a template. PARP3 cDNA (Image clone ID: 4763951; Open Biosystems) was amplified using following primers: 5′ GGA ATT CGA TGG CTC CAA AGC CG 3′ and 5′ GGG GTA CCG AGG TGG ACC TCC AG 3′, and the amplified polymerase chain reaction product was then cloned into pEGFP-C1 at EcoRI and KpnI, creating pEGFP-PARP3. The pGEX4T3-$APLF^{WT}$, pGEX4T3-$APLF^{FHA}$, pGEX4T3-$APLF^{R27A}$, pGEX4T3 $APLF^{PBZ1/2}$ and pGEX4T3-$APLF^{PBZ1/2m}$ constructs were created as previously described (18,20). To generate pBABE-puro-eCFP for usage in the plasmid integration assay, pECFP-C1 (Clontech) was digested with ApaLI and AflII, blunt-ended and ligated in-frame into the EcoRI site of pBABE-puro (Clontech). The pSUPER.retro.neo + GFP plasmid was used for expressing the APLF RNAi sequence GAAGAAATCTGCAAAGATA. A pSUPER RNAi-resistant APLF rescue construct harbouring six different nucleotides in the RNAi target sequence GAGGAGATTTGTAAGGAC (changed nucleotides are underlined) was generated by Quikchange site-directed mutagenesis (Stratagene) in the indicated plasmids to create pcDNA3.1/V5-$APLF^{WT}$ and pEGFP-$APLF^{WT}$ siRNA-resistant constructs. Quikchange site-directed mutagenesis (Stratagene) was then used to create pcDNA3.1/V5-$APLF^{S116A}$ and pcDNA3.1/V5-$APLF^{S116D}$ RNAi-resistant plasmids using RNAi-resistant pcDNA3.1/V5-$APLF^{WT}$ plasmid as a template. All plasmid constructs and site-directed mutagenesis were verified by sequence analysis.

Cell culture and transfections

U2OS and HEK293T cell lines were cultured in Dulbecco's Modified Eagle Medium supplemented with 10% fetal bovine serum, 50 U/ml penicillin, 50 μg/ml streptomycin and were maintained at 37°C in a humidified atmosphere containing 5% CO_2. U2OS cell lines stably expressing EGFP-APLF, EGFP-$APLF^{S116A}$ and EGFP-$APLF^{S116D}$ were generated as previously described (20). Stably depleted APLF U2OS (U2OS-$APLF^{KD}$) cells were established by transfecting pSUPER vector or pSUPER vector encoding the APLF RNAi sequence (described earlier in the text) (18,22), selected with 800 μg/ml of G418 (Gibco) and maintained with 200 μg/ml G418. To establish $U2OS^{EGFP\text{-}APLF}$ cells (U2OS-$APLF^{KD}$ cells stably expressing EGFP-APLF), U2OS-$APLF^{KD}$ cells were transfected with 2 μg of siRNA-resistant EGFP-$APLF^{WT}$ and placed under selective pressure with 800 μg/ml of G418 (Gibco) and 200 μg/ml puromycin (Sigma). Resistant colonies were isolated and maintained with 200 μg/ml of G418 (Gibco) and 200 μg/ml puromycin (Sigma). G_0/G_1 synchronized cells were established by plating cells at a concentration of 4.5×10^5 cells/35-mm plate until confluency. Once confluent, cells were cultured further for an additional 2 days before treatment. Synchronized cells were then stained and visualized using the 5-ethynyl-2′-deoxyuridine (EdU)-labelling immunofluorescence kit, as described later in the text. Transfections were performed with the Effectene transfection kit (Qiagen) or, for siRNA treatments, with DharmaFECT 1 transfection reagent (Dharmacon) according to the manufacturer's instructions. All pooled siRNAs were purchased from Dharmacon.

Antibodies

Anti-pSer^{116}-APLF polyclonal antibodies were generated by immunizing New Zealand white rabbits using keyhole limpet hemocyanin-conjugated Ser^{116} phosphopeptide (CLRN(pS)QVLDEDKK) according to standard immunological protocols. Antibodies Inc. provided the injection of rabbits and production bleeds. The pSer^{116}-APLF antibody was affinity purified using negative and positive selections with the non-phosphorylated and phosphorylated APLF peptides, respectively. The production of the anti-APLF antibody has been previously described (18). Commercial antibodies used in this study were from Invitrogen (V5), Cell Signaling Technology (PARP1), LifeSpan BioSciences (PARP2), Alexis Biochemicals (PARP3), Santa Cruz Biotechnology (GFP, GST and tubulin), Serotec (XRCC4), Upstate (γH2AX), Abcam (actin, ATM, DNA-PKcs-Ser(P)^{2056}), Trevigen (PAR) and Epitomics Inc. (ATM-Ser(P)^{1981}).

Expression and purification of fusion proteins

APLF recombinant proteins were produced in *Escherichia coli* BL21(DE3)/pLysS (Novagen). For the purification of the GST-fusion proteins, bacteria were grown to an OD 600 of 0.6, and expression was induced by addition of 0.2 mM isopropylthio-β-galactoside (IPTG) for 3 h at 30°C. Cells were lysed in a buffer containing 20 mM Tris–HCl (pH 8.0), 0.5 M KCl, 20 mM imidazole (pH 7.0), 5 mM β-mercaptoethanol, 10% glycerol, 0.2% Tween-20 and 1 mM phenylmethylsulfonyl fluoride (PMSF) and purified on GST beads according to the manufacturer's instructions (Qiagen).

Preparation of cell extracts, immunoprecipitation, pull-downs and immunoblotting

Whole-cell extracts (WCEs) were prepared from the indicated cell lines as previously described (23). Cells were irradiated with a MDS Nordion Gammacell 40 Irradiator (^{137}Cs source) at a dose rate of 0.88 Gy per minute and then incubated at 37°C as indicated before lysis. For Ultraviolet (UV)-C radiation treatment, cultured cells were washed once with phosphate buffered saline and then UV irradiated (25 J/m^2) with using UV Stratalinker 2400 (Stratagene) in the presence of phosphate buffered saline. Following UV irradiation, cells were placed again in culture media and incubated at 37°C for 1 h until cell harvest. Etoposide (25 μM; VP16), camptothecin (2 μM), methyl methanesulfonate (4 mM; methyl methanesulfonate), hydroxyurea (1 mM; HU) and hydrogen peroxide (0.5 mM; H_2O_2) were purchased from Sigma. Cell extract preparation, immunoprecipitations and immunoblotting were performed as previously described (23). Cells were pretreated for 1 h with inhibitors to ATM (10 μM KU55933; Calbiochem) or to DNA-PKcs (1 μM NU7441; Selleck Chemicals) or the PARP inhibitors PJ-34 (10 μM; Sigma-Aldrich), ABT888 (10 μM; Selleck Chemicals) or AZD2281 (2.5 μM; Selleck Chemicals) where indicated. For immunoblotting experiments examined with LI-COR, IRDye infrared secondary antibodies were cross-adsorbed for multiplex detection, and the antibody conjugates were assessed on a LI-COR Odyssey imaging system. Pull-down assays were performed as previously described (18).

Chromatin isolation

Chromatin fractionations were carried out using a sub-cellular protein fractionation kit (Thermo Scientific), according to the manufacturer's instructions.

Colony formation assay

Clonogenic survival assays were performed as previously described (24).

Immunofluorescence microscopy

Cells were imaged using the widefield setting of an Olympus IX81 by multichannel 3D acquisition controlled with Metamorph software (MDS Analytical Technologies). Cells were viewed using a PLAPON 60 × 1.42NA oil-immersion objective and imaged with a Photometrics Cascade 512B EM-CCD camera (Roper Scientific) yielding images with 0.27 mm × 0.27 mm pixels and 0.25 mm steps through Z. Raw images were deconvolved using 25 iterations of 3D-blind deconvolution (Autoquant, Media Cybernetics). Foci quantification was performed by eye. Cells undergoing DNA replication were visualized using EdU labelling. Staining for EdU was done using a Click-iT EdU 647 Alexa Fluor Imaging kit according to manufacturer's specifications (Invitrogen). EdU at 10 μM was added 1 h before fixation of cells.

Laser microirradiation and time-lapse imaging

Two-photon laser microirradiation was performed with U2OS cell lines as indicated, in fresh culture medium placed on the stage (heated at 37°C) of a Zeiss LSM510 NLO laser-scanning confocal and two-photon microscope, and the fold increase in fluorescence intensity following laser microirradiation as a function of time over the 5-min time-lapse was quantified as previously described (20). Fluorescence intensity following laser microirradiation as a function of time for the 30-min period was quantified using ImageJ software (NIH). Quantification of fluorescence intensity following laser microirradiation was normalized to background fluorescence to account for potential photo-bleaching.

Random plasmid integration assay

Random plasmid integration assay was performed essentially as described (18,25) with some modifications. U2OS-APLF^{KD} cells were transfected with empty vector, pSUPER RNAi-resistant APLF^{WT}, RNAi-resistant APLF^{S116A} or RNAi-resistant APLF^{S116D} and incubated for 48 h at 37°C. Throughout experimentation, the expression levels of the APLF proteins in the APLF-depleted U2OS cells were verified by immunoblotting. Subsequently, cells were transfected with linearized pBABE-puro-eCFP plasmid DNA containing a puromycin resistance cassette. Twenty-four hours later, cells were replated at low density in selective media containing 2 μg/ml puromycin and incubated for 10 days at 37°C.

Colonies were then stained with Coomassie Blue dye and counted. A fraction of the transfected cells was monitored for nuclear eCFP expression to normalize the data for transfection efficiency. The relative plasmid integration of the APLF-depleted cell lines reconstituted with RNAi-resistant APLF^{WT} was set at 100% integration. The error bars represent the standard error of the mean. Three independent experiments were performed in triplicate. Transient transfections were performed with the Effectene transfection kit (Qiagen) according to the manufacturer's instructions.

RESULTS

ATM-dependent phosphorylation of APLF at Ser^{116} *in vivo*

Many DDR proteins undergo functionally important post-translational modifications in response to DNA damage. In keeping with this, APLF undergoes IR-induced and ATM-dependent phosphorylation (18,22,26). Site-directed mutagenesis studies have identified the primary site of ATM-dependent phosphorylation at Ser^{116} (18,26), and APLF is directly phosphorylated by ATM at Ser^{116} *in vitro* (Supplementary Figure S1A). To further characterize the role of APLF Ser^{116} phosphorylation *in vivo*, we developed a phospho-specific antibody directed against an APLF Ser^{116} phosphopeptide and examined the phosphorylation of APLF at Ser^{116} following exposure to IR in U2OS cells. Our anti-pSer^{116} APLF antibody demonstrated immunoreactivity on western blotting to a band corresponding to the apparent molecular weight of endogenous APLF following exposure to IR (Figure 1A), which was not detected when APLF levels were depleted by siRNA (Figure 1B). Furthermore, the APLF pS116 antibody recognized V5-tagged WT APLF ectopically expressed in HEK293T cells following treatment with IR, but did not appreciably detect WT APLF under basal conditions or the mutant protein harbouring a substitution of Ser^{116} to alanine (APLF^{S116A}), as judged by western blotting (Figure 1C). These data suggest that the pSer^{116}-APLF antibody is specific for the phosphorylated APLF Ser^{116} epitope.

We next examined U2OS cells stably expressing EGFP-APLF and found that following exposure to a variety of DNA damaging agents only those known to activate ATM [IR, hydrogen peroxide (H_2O_2), camptothecin (CPT), etoposide (VP16) and methyl methanesulfonate] induced phosphorylation at Ser^{116} (Figure 1D). In contrast, UV-C radiation, which is known to specifically activate ATR, but not ATM (27), did not result in detectable Ser^{116} phosphorylation (Figure 1D). Similarly, prolonged treatment with 1 mM hydroxyurea (HU) did not result in APLF-Ser^{116} phosphorylation (Figure 1D, Supplementary Figure S1B). The level of Ser^{116} phosphorylation from U2OS cells stably expressing EGFP-APLF^{WT} was observed as early as 1 min following 10 Gy γ-IR, peaked within the first hour and returned to pre-irradiation levels by 24 h (Supplementary Figure S1C).

As many of the DNA damaging agents that led to the phosphorylation of APLF-Ser^{116} are known to activate both the ATM and DNA-PKcs protein kinases, APLF-Ser^{116} phosphorylation was also examined in the presence of ATM and DNA-PKcs inhibition. As judged by anti-pSer^{116}-APLF western blotting, phosphorylation levels were virtually abolished in the presence of ATM inhibition, but not with DNA-PKcs inhibition (Figure 1E). We additionally noted that on occasion, a low level of basal APLF-Ser^{116} phosphorylation was detected, particularly in WCEs from HEK293T cells transiently transfected with pEGFPC2-APLF^{WT} (Figure 1F). A low level of endogenous APLF-Ser^{116} phosphorylation was not typically observed under basal conditions (Figure 1A). Therefore, it is possible that the transient transfection itself contributed to the phosphorylation of WT EGFP-APLF at Ser^{116} detected in the absence of DNA damage (Figure 1F).

The APLF PBZ domains and PARP3 modulate the IR-induced phosphorylation of APLF at Ser^{116}

APLF has been shown to be recruited to laser-induced DNA lesions, and to interact with PAR, in a PBZ-dependent manner (20). Therefore, we wondered whether there might be a relationship between pSer^{116}-APLF and the APLF PBZ domains. To further investigate this, we initially compared the IR-induced pSer^{116}-APLF levels of U2OS cell lines stably expressing WT EGFP-APLF with those expressing the EGFP-tagged APLF PBZ mutant proteins, APLF^{PBZ1m} and APLF^{Y381A}, which are known to disrupt PAR-binding and abolish the recruitment of APLF to sites of laser-induced DNA damage (20). Indeed, we found that both APLF^{PBZ1m} and APLF^{Y381A} were associated with diminished levels of pSer^{116}-APLF as judged by western blotting (Figure 1F). Interestingly, when we examined the IR-induced pSer^{116} of another APLF mutant, APLF^{PBZ2m}, which is associated with a less severe PAR-binding and recruitment defect (20), we found that the phosphorylation of Ser^{116} was less impaired relative to the APLF^{PBZ1m} and APLF^{Y381A} mutant proteins (Figure 1F).

We next examined the IR-induced phosphorylation of APLF following pre-treatment with a variety of PARP inhibitors (PJ-34, ABT888 and AZD2281) (Figure 1G). Interestingly, only pre-treatment with the PARP inhibitor AZD2281 significantly reduced IR-induced levels of pSer^{116}-APLF, while neither pre-treatment with PJ-34 or ABT888 had any appreciable effect. At the concentrations used in these experiments, all three of the PARP inhibitors are expected to have a strong inhibitory effect on both PARP1 and PARP2. We wondered then why only AZD2281 treatment was associated with impaired APLF-Ser^{116} phosphorylation. Different PARP inhibitors have been shown to display varying selectivity towards PARP3 (28) and, in general, demonstrate less potency against PARP3. However, the PARP inhibitor KU0058948 is a relatively active PARP3 inhibitor (28) and is structurally similar to AZD2281. Therefore, we speculated that the PBZ-dependent phosphorylation of

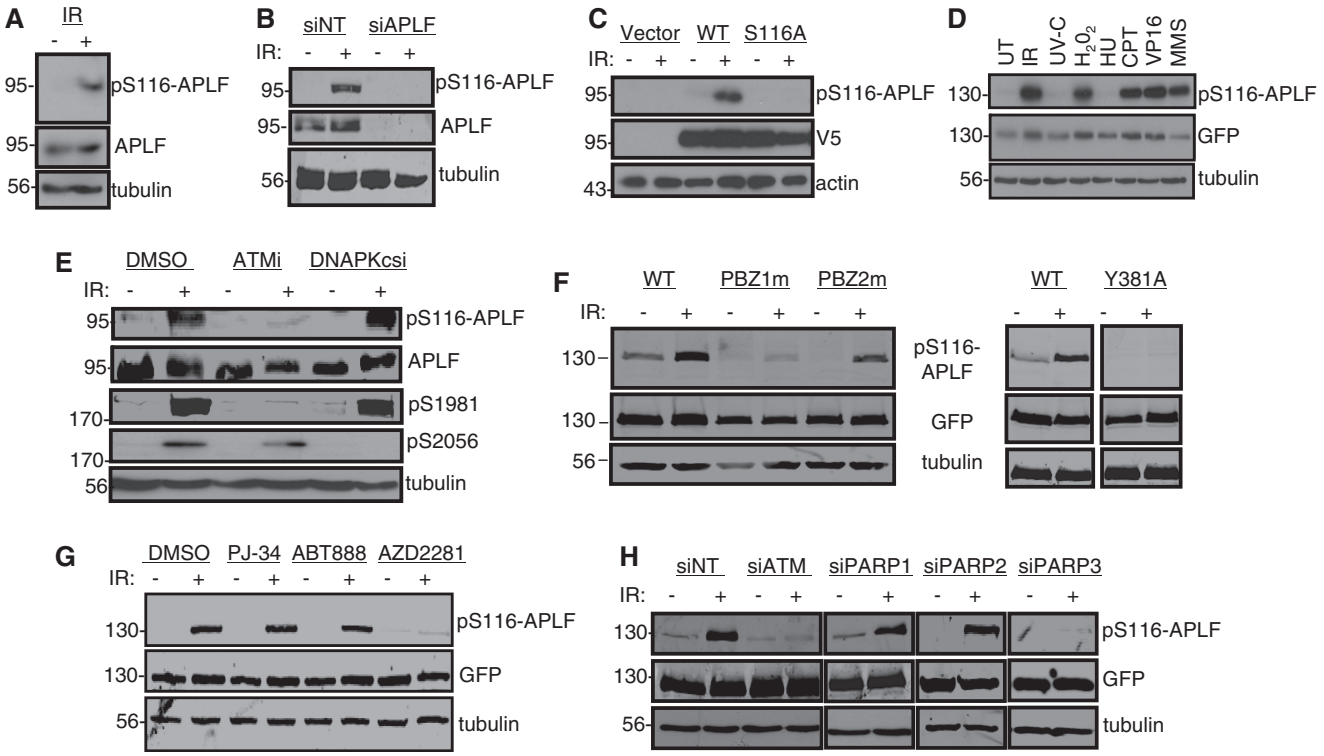

Figure 1. APLF undergoes IR-induced ATM- and PAR/PBZ-dependent phosphorylation at Ser^{116}. (**A**) U2OS cells were mock or irradiated with 10 Gy γ-rays, WCEs were harvested 1 h later and immunoblotted with the antibodies as indicated. (**B**) HEK293T cells were transfected with siRNA against APLF (siAPLF), or non-targeting siRNA control (siNT), and 72 h later were mock or irradiated with 10 Gy γ-rays. WCEs were harvested 1 h later and prepared and immunoblotted with the antibodies as indicated. (**C**) HEK293T cells transiently expressing empty vector, V5-tagged APLF^{WT} or APLF^{S116A}, were treated with or without 10 Gy γ-IR. WCEs were harvested 30 min later and immunoblotted with antibodies as indicated. (**D**) U2OS cells expressing EGFP-APLF^{WT} were treated as indicated. WCEs were harvested 30 min later and immunoblotted with the antibodies as specified. UT, untreated control; IR, 10 Gy γ-rays. (**E**) HEK293T cells were pre-treated as indicated for 1 h and then subjected to mock or 10 Gy IR. WCEs were harvested 30 min later and immunoblotted with antibodies as indicated. The pS1981 and pS2056 correspond to ATM and DNA-PKcs phospho-specific antibodies. (**F**) HEK293T cells transiently expressing EGFP-tagged APLF^{WT}, APLF^{PBZ1m}, APLF^{PBZ2m} and APLF^{Y381A} were treated with or without 10 Gy γ−IR. WCEs were harvested 1 min following IR and immunoblotted with the antibodies as indicated. (**G**) U2OS cells stably expressing EGFP-APLF^{WT} were pre-treated with the chemical inhibitors as indicated, 1 h before 6 Gy γ-IR. WCEs were harvested 1 min following IR and immunoblotted with the indicated antibodies. (**H**) U2OS cells stably expressing EGFP-APLF were transfected with NT, ATM, PARP1, PARP2 or PARP3 siRNA 72 h before 6 Gy γ-IR. Cells were harvested 1 min following IR, and WCEs were immunoblotted with antibodies as indicated.

APLF-Ser^{116} might be facilitated by PARP3. To further investigate this, U2OS cells stably expressing EGFP-APLF were depleted of PARP3, as well as PARP1 or PARP2 using siRNA. The depletion of PARP1 or PARP2 did not reduce the level of pAPLF-Ser^{116} following IR appreciably, whereas the depletion of PARP3 resulted in undetectable pSer^{116}-APLF, similar to what was observed following siRNA-mediated depletion of ATM (Figure 1H, Supplementary Figure S2A). To ensure that the siRNA-mediated depletion of PARP1, PARP2 or PARP3 was specific for each PARP, levels of the PARPs were examined from all three PARP siRNA treatments by western blotting, which confirmed the specificity of the siRNA-mediated knockdowns (Supplementary Figure S2B). As an additional measure, U2OS-expressing EGFP-APLF cells were depleted of XRCC4, which, in contrast to ATM and PARP3, has been shown to function downstream of APLF in the DDR (15), and pAPLF-Ser^{116} levels were assessed by western blotting (Supplementary Figure S3A). Consistent with a role downstream of APLF, XRCC4 depletion had no measurable effect on IR-induced APLF-Ser^{116} phosphorylation. Lastly, U2OS$^{EGFP-APLF}$ cells stably expressing EGFP-APLF at a level comparable with that of endogenous APLF (Supplementary Figure S3B) were used to facilitate the immunofluorescence analysis of the effects of the various PARP inhibitors on the IR-induced co-localization of pSer^{116}-APLF with γH2AX foci. As demonstrated in Figure 2A, there was a dramatic reduction of pSer^{116}-APLF IR-induced foci with AZD2281 pretreatment, but no difference was noted between the vehicle control and ABT888 or PJ-34 pretreatment.

PARP3 and APLF interact in a PBZ-dependent manner

As the depletion of PARP3 compromised APLF-Ser^{116} phosphorylation following IR, we next examined the interaction between PARP3 and APLF. First, the effects of whole cell irradiation of U2OS$^{EGFP-APLF}$ cells were examined, which demonstrated partial IR-induced

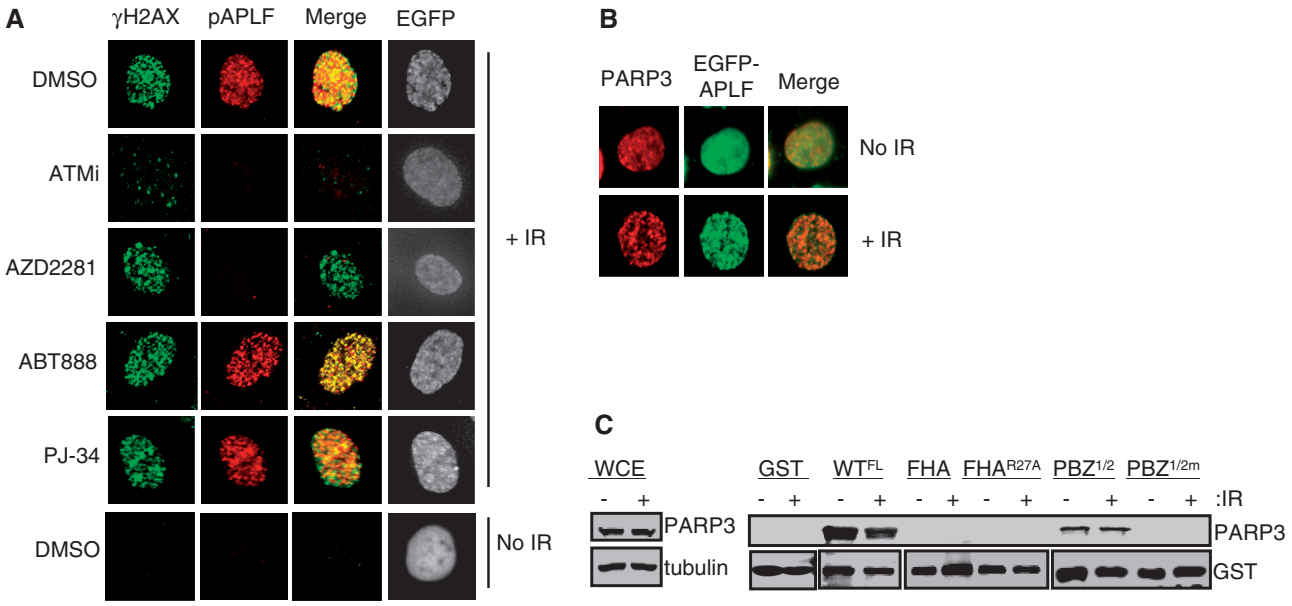

Figure 2. APLF and PARP3 co-localize and PARP3 is required for APLF-pSer^{116}. (**A**) U2OS cells stably depleted of APLF and stably reconstituted with RNAi-resistant EGFP-APLF^{WT} were pre-treated as indicated for 1 h before 2 Gy γ-IR, then fixed 30 min later and stained with the indicated antibodies. (**B**) The U2OS cells from 2A were treated with or without 2 Gy γ-IR, fixed immediately and stained for PARP3. EGFP and PARP3 images were merged as indicated. (**C**) HEK293T cells treated with or without 6 Gy γ-IR were harvested immediately following γ-IR, incubated with the various immobilized GST-APLF peptides, then examined by anti-PARP3 or anti-GST immunoblotting.

co-localization between PARP3 and EGFP-APLF^{WT} (Figure 2B). We next performed pull-down experiments using various portions of APLF fused to GST as bait and mixed WCEs from mock or irradiated HEK293T cells to identify interactions with endogenous PARP3 (Figure 2C). We demonstrated a PBZ-dependent APLF-PARP3 interaction (Figure 2C), which is consistent with a reported PAR-dependent interaction between APLF and PARP3 (15). However, we wondered whether IR might induce additional FHA-dependent interactions between these proteins, as PARP3 is predicted to have PIKK consensus sites of threonine phosphorylation (http://scansite.mit.edu/). Thus, alongside the immobilized GST-PBZ1/2^{WT} and GST-PBZ1/2 m APLF peptides, we included GST-FHA^{WT} and the APLF FHA mutant domain, GST-FHA^{R27A} (Figure 2C). The results shown in Figure 2C suggest that PARP3 and APLF interact independently of the APLF^{FHA} domain, and that this interaction can occur both basally and following IR in a PBZ-dependent manner.

ATM and PARP3 modulate the recruitment of APLF to laser-induced DNA damage

As PARP3 both interacts with APLF and is necessary for the phosphorylation of APLF-Ser^{116}, we next questioned whether PARP3 might also be involved in the recruitment of APLF to laser-generated sub-nuclear damage. To examine this, we used two-photon laser microirradiation. Laser microirradiation is advantageous for its ability to generate DNA damage within a defined sub-nuclear volume, and, by examining live cells, the spatiotemporal analyses and kinetics can be performed without the requirement for cellular fixation and immunostaining procedures. In addition, laser microirradiation induces protein redistribution that qualitatively and quantitatively resembles 'classical' IR-induced foci (29). We have previously compared independently isolated U2OS cell lines stably expressing different levels of EGFP-APLF and showed that the recruitment to sites of laser-induced DNA damage is not significantly affected by EGFP-APLF levels (20). Furthermore, using this method for laser microirradiation and real-time imaging analysis, we and others have demonstrated that the recruitment of EGFP-APLF to laser tracks is dependent on PAR synthesis (20,30). Additionally, PAR, γH2AX and pSer^{116}-APLF were detected at the laser tracks by immunostaining (Figure 3A).

We next monitored the recruitment kinetics of EGFP-APLF^{WT} stably expressed in U2OS cells that were either depleted of PARP1, PARP2, PARP3 or ATM by siRNA, or pre-treated with PARP inhibitors as indicated (Figure 3B and C, Supplementary Figure S4). The depletion of PARP1 and PARP2, as well as pre-treatment with the PARP inhibitors PJ-34 and AZD2281, had very strong inhibitory effects on the initial recruitment of EGFP-APLF to the laser tracks. The siRNA-mediated depletion of PARP3 (siPARP3) also impaired the recruitment of EGFP-APLF but less severely than that observed with EGFP-APLF recruitment in cells depleted of PARP1 or PARP2 (Figure 3B and C). Similarly, the depletion of PARP1 by siRNA demonstrated a more deleterious effect than siPARP3 on the association of APLF^{WT} with irradiated chromatin at 5 min (13 and 27%, respectively) (Figure 3D, Supplementary Figure S5). Interestingly, the cells depleted of ATM or PARP3 exhibited very similar impairment of EGFP-APLF recruitment kinetics.

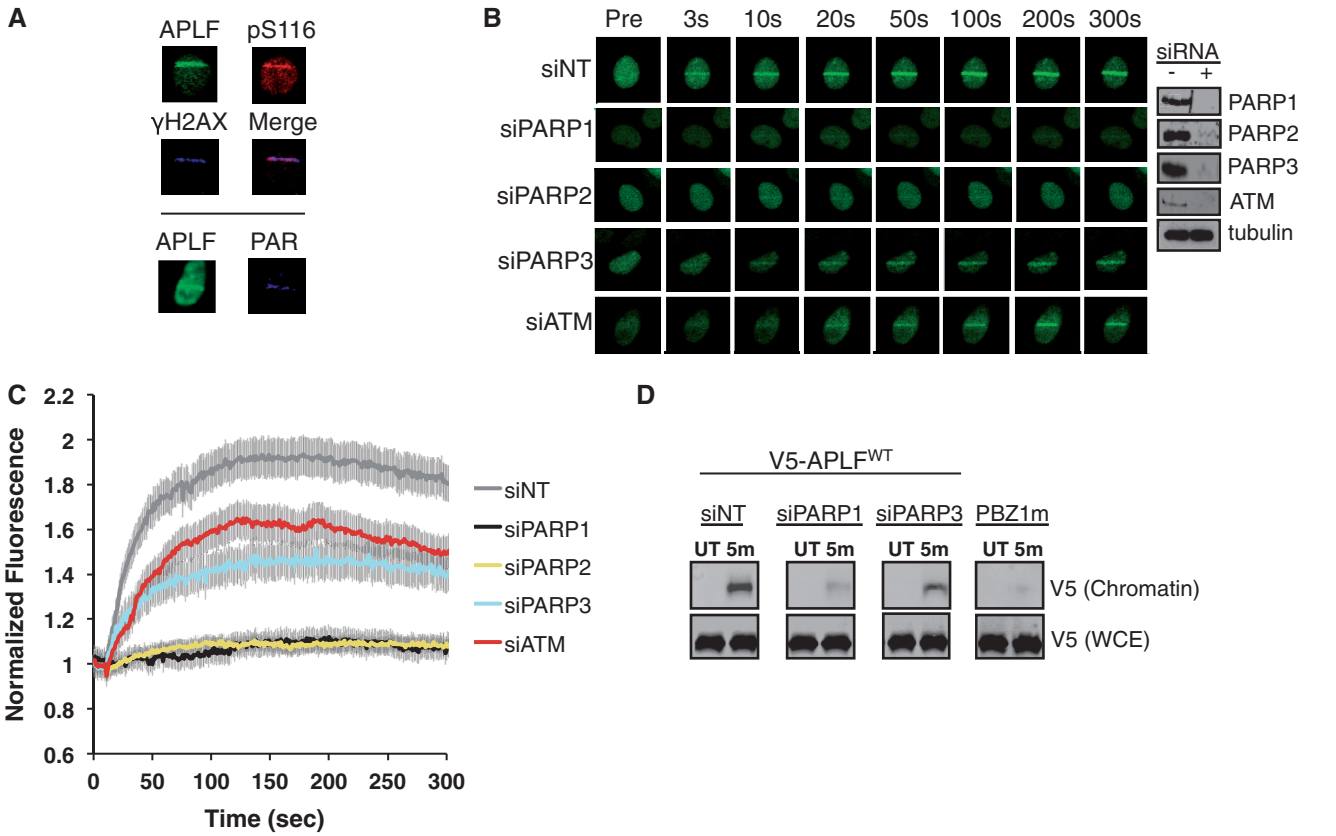

Figure 3. PARP3 and ATM-dependent phosphorylation of APLF-Ser^{116} influence the kinetics of APLF at laser-induced DNA damage. (**A**) EGFP-APLF (GFP) accumulation at the laser tracks was examined by fluorescence microscopy, U2OS cells were subsequently fixed 30 min following damage and stained as indicated. (**B**) U2OS cells stably expressing EGFP-APLF^{WT} were pretreated for 72 h with either NT, PARP1, PARP2, PARP3 or ATM siRNA and subjected to two-photon laser-microirradiation coupled with live cell time-lapse imaging over 5 min. Control western blots for the specific siRNA targeted depletion of PARP1, PARP2, PARP3 or ATM. (**C**) Quantification of the recruitment kinetics of EGFP-APLF examined in 3B. Error bars represent the standard error of the mean (SEM). **(D)** HEK293T cells transiently expressing V5-APLF^{WT} were pretreated with, or without, the indicated siRNA for 72 h prior to 10 Gy γ-IR, and were harvested 5 min later. HEK293T cells expressing V5-APLF^{PBZ1m} were analyzed in parallel as a control. WCEs and chromatin fractions were immunoblotted with the antibodies as indicated.

When the time course analysis was extended to 15 min, we found that EGFP-APLF was present at the tracks in cells pretreated with PJ-34 but could not be observed in cells pretreated with AZD2281 (Supplementary Figure S6). Furthermore, Ser^{116} phosphorylation was detected at the tracks by immunostaining following treatment with PJ-34 and was similar to the levels quantified for the vehicle control (DMSO). No pSer^{116} was detected following AZD2281 treatment (Supplementary Figure S6).

ATM inhibition impairs PARP3 recruitment

The similar effects of ATM or PARP3 depletion on EGFP-APLF recruitment, as well as on IR-induced pSer^{116}-APLF levels, led us to wonder whether ATM and PARP3 might be involved in a related signalling pathway with APLF. PARP3 recruitment has been previously shown to be unaffected by PARP inhibition (KU0058948) (17), suggesting that the assembly of PARP3 at sites of DNA damage does not depend on PAR synthesis. In contrast, U2OS cells expressing EGFP-PARP3 that had been pre-treated with ATM inhibitor (KU55933) then subjected to laser-induced sub-nuclear damage demonstrated a profound defect in EGFP-PARP3 recruitment to the laser tracks (Figure 4A, Supplementary Figure S7A and B). However, depletion of PARP3 did not appreciably affect damage-induced ATM kinase activity, as we detected phosphorylation of the ATM autophosphorylation residue, Serine-1981 following IR (Figure 4B). Furthermore, ATM inhibition had no measurable effect on EGFP-PARP1 recruitment in U2OS cells (Supplementary Figure S7C). When the combined treatment of ATM inhibition and PARP3 depletion on EGFP-APLF recruitment in U2OS cells was monitored, the combination was found to be indistinguishable from the effects of the individual treatments of either ATM inhibition or PARP3 depletion (Figure 4C, Supplementary Figure S8). Collectively, these data are consistent with the notion that ATM and PARP3 function in a common pathway to modulate APLF-Ser^{116} phosphorylation and APLF recruitment kinetics.

Phosphorylation of APLF-Ser^{116} increases the association of APLF at sites of DNA damage

As the phosphorylation by ATM of downstream targets has been shown to facilitate the association of specific DDR proteins with chromatin following DNA damage

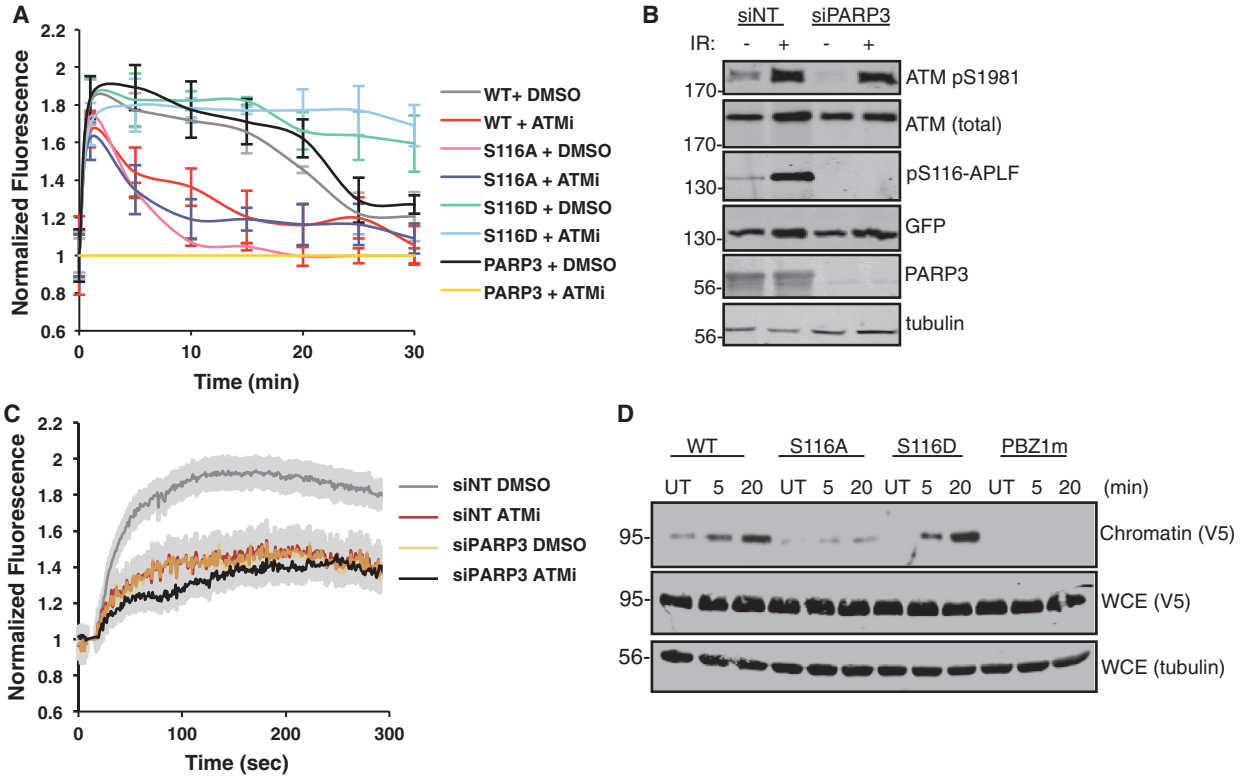

Figure 4. Combined PARP3 depletion and ATM inhibition do not result in additive impairment in EGFP-APLF accumulation at DNA lesions. (**A**) U2OS cells expressing EGFP-APLF^{WT}, EGFP-APLF^{S116A}, EGFP-APLF^{S116D} or EGFP-PARP3 were subjected to two-photon laser-microirradiation coupled with live cell time-lapse imaging over 30 min in the presence of DMSO or ATM inhibitor and quantified. At least ten cells were examined per treatment. Error bars, SEM. (**B**) U2OS cells stably expressing EGFP-APLF^{WT} were pretreated with either NT or PARP3 siRNA for 72 h prior to 6 Gy IR. WCEs were harvested immediately following treatment and immunoblotted with the antibodies as indicated, to confirm the depletion of PARP3 as well as the phosphorylation status of the indicated proteins. (**C**) U2OS cells stably expressing EGFP-APLF^{WT} were pretreated for 72 h with either NT or PARP3 siRNA. One hour prior to laser microscopy, cells were incubated with DMSO or ATM inhibitor and then subjected to two-photon laser-microirradiation coupled with live cell time-lapse imaging over 5 min. At least ten cells were examined per treatment and fluorescent intensities were quantified. Error bars, SEM. At least eight cells were examined per treatment. (**D**) HEK293T cells transiently expressing V5-APLF^{WT}, V5-APLF^{S116A}, V5-APLF^{S116D} or V5-APLF^{PBZ1m} were subjected to 10 Gy γ-IR and harvested at the indicated times. WCEs and chromatin fractions were immunoblotted with the antibodies as indicated.

(9,10), we sought to examine the impact of APLF-pSer^{116} on APLF recruitment and accumulation kinetics. To do so, U2OS cells stably expressing EGFP-APLF^{WT}, EGFP-APLF^{S116A} or EGFP-APLF^{S116D} were examined using laser micro-irradiation and live cell time-lapse imaging for 30 min (Figure 4A, Supplementary Figure S7A). Following the rapid accumulation of EGFP-APLF to sites of laser-induced DNA damage, we noticed a decline in the accumulation of the EGFP-APLF^{WT} protein after 20 min, which was further decreased by ATM inhibition. When we then compared WT-APLF recruitment kinetics with the phospho-ablative mutant (EGFP-APLF^{S116A}), we found that the accumulation of EGFP-APLF^{S116A} at laser tracks beyond 5 min was substantially reduced compared with EGFP-APLF^{WT} and was similar to the kinetics observed for EGFP-APLF^{S116A} in the presence of ATM inhibition. In contrast, the phospho-mimicking mutant (EGFP-APLF^{S116D}) was found to restore accumulation at the laser tracks to WT levels in the presence or absence of ATM inhibition (Figure 4A, Supplementary Figure S7A). Similarly, when U2OS cells stably expressing EGFP-tagged APLF^{WT}, APLF^{S116A} or APLF^{S116D} were depleted of PARP3 by siRNA, only APLF^{S116D} rescued the accumulation at 20 and 30 min (Supplementary Figure S9).

To further examine the relationship between APLF retention at chromatin and ATM-dependent APLF^{S116} phosphorylation, chromosomal fractionation experiments were performed following whole-cell irradiation of U2OS cell lines expressing V5-tagged APLF^{WT}, APLF^{S116A}, APLF^{S116D} or APLF^{PBZ1m} (Figure 4D, Supplementary Figure S10A) and U2OS cell lines expressing V5-tagged APLF^{WT} pre-treated with the ATM inhibitor KU55933 (Supplementary Figure S10B). We found that the level of APLF^{S116A} was decreased in the irradiated chromosomal fraction compared witrh APLF^{WT} or APLF^{S116D} most notably at 20 and 30 min following irradiation (Figure 4D, Supplementary Figure S10A). Similarly, 20 min following irradiation, the amount of APLF^{WT} associated with chromatin was reduced in the presence of ATM inhibition by 48% (Supplementary Figure S10B and C). The PAR-binding mutant control, APLF^{PBZ1m}, displayed decreased levels of APLF associated with

chromatin at all measured times following irradiation (Figure 4D).

APLF-S116A is associated with increased residual DSBs following IR and cellular radiosensitivity

To address the biological significance of APLF^{S116} phosphorylation, we examined the effect of the APLF^{S116A} phospho-mutant on DSB repair kinetics. Confluent and non-dividing U2OS cells stably depleted of APLF by shRNA (U2OS-APLF^{KD}) and reconstituted with empty vector, RNAi-resistant and V5-tagged APLF^{WT}, APLF^{S116A} or APLF^{S116D}, were subjected to 2 Gy γ-IR, and residual γH2AX foci were measured at the indicated recovery periods (Figure 5A). Compared with the U2OS-APLF^{KD} cells reconstituted with WT APLF or APLF^{S116D}, significantly more γH2AX foci were observed in the cells that had been reconstituted with empty vector or APLF^{S116A}, most notably at 4 and 24 h following IR (Figure 5A).

As APLF has been shown to be involved in NHEJ (15,18), we wondered whether Ser^{116} phosphorylation might play a role in APLF-dependent NHEJ. NHEJ is known to be required for the random plasmid integration of plasmid DNA into the genome of cells in culture and has been used previously as a measure of APLF-dependent NHEJ (18). Therefore, we examined the efficiency of random plasmid integration in U2OS-APLF^{KD} cells that had been reconstituted with RNAi-resistant WT-APLF, APLF^{S116A} or APLF^{S116D} (Figure 5B). We found that cells expressing APLF^{S116D} rescued APLF-dependent NHEJ close to WT levels, whereas U2OS-APLF^{KD} cells expressing APLF^{S116A} demonstrated a significant reduction in plasmid integration efficiency to ~60% that of WT-APLF (Figure 5B). We also examined the contribution of APLF-Ser^{116} phosphorylation on the association of the downstream NHEJ factor, XRCC4, with chromatin (Supplementary Figure S10A and D). To assess this, chromatin fractionation experiments were performed from cells expressing APLF^{WT}, APLF^{S116A} and APLF^{S116D}, and XRCC4 levels were monitored (Supplementary Figure S10A). We observed a 44% reduction in the association of XRCC4 with irradiated chromatin at 30 min in cells expressing APLF^{S116A} compared with APLF^{WT} and APLF^{S116D} (Supplementary Figure S10D), suggesting that APLF Ser^{116} phosphorylation contributes to the stability of XRCC4 at damaged chromatin.

Lastly, clonogenic survival assays were performed to establish whether APLF-Ser^{116} phosphorylation might play a role in cellular radioresistance. Reconstituted U2OS-APLF^{KD} cells were again reconstituted with RNAi-resistant WT-APLF, APLF^{S116A} or APLF^{S116D}, exposed to increasing doses of γ-IR, and clonogenic survival was measured (Figure 5C). We found that the U2OS-APLF^{KD} cells expressing APLF^{S116A} displayed increased radiosensitivity compared with cells reconstituted with either WT-APLF or APLF^{S116D}, suggesting that cellular survival is dependent on APLF-Ser^{116} phosphorylation.

DISCUSSION

It has been well described that the APLF PBZ domains interact with PAR, and that this interaction is critical for the initial and rapid recruitment of APLF to laser-induced DNA lesions (18–20). It has similarly been reported that APLF undergoes ATM-dependent phosphorylation at Ser^{116} (26). However, the function or means by which this phosphorylation occurs had not been previously assessed. Therefore, we sought to examine the biological significance of APLF Ser^{116} phosphorylation.

Activated ATM is recruited into foci at sites of DNA damage (31), where it then phosphorylates several DDR substrates, including H2AX at Ser^{139} or γ-H2AX (32), and the phosphorylation of these proteins by ATM is often associated with their recruitment and association at damaged DNA (9,10,32,33). Consistent with this, we found that the interaction of APLF at DNA damage sites also appears to be dependent on the phosphorylation of amino acid residue Ser^{116}. The APLF-S116A mutant was barely detectable in the irradiated chromatin fraction at, or after 20 min, whereas the phospho-mimetic mutant APLF-S116D was unaffected and restored interactions with the chromosomal fraction to WT levels (Figure 4D, Supplementary Figure S10A). The accumulation of APLF at sites of laser-induced DNA damage was also dependent on Ser^{116} phosphorylation (Figure 4A, Supplementary Figure S7A), and IR induced the co-localization of phosphorylated APLF-Ser^{116} with γH2AX foci (Figure 2A). Therefore, the data strongly suggest that the phosphorylation of APLF appears to be important for facilitating DSB damage signalling and repair. However, the precise mechanism by which this occurs is not clear, although it is possible that Ser^{116} phosphorylation induces a conformational change and/or directs phospho-dependent interactions between APLF and downstream effectors. In addition, we cannot rule out the possibility that there are other sites of PIKK-dependent phosphorylation, which might contribute to some aspect of APLF function. However, within the context of our studies, it seems unlikely that there are additional sites of ATM-dependent phosphorylation that impact on APLF accumulation, as ATM inhibition did not alter the retention kinetics of APLF-S116A at sites of laser-generated DNA damage (Figure 4A, Supplementary Figure S7A).

The phosphorylation of other factors involved in the DDR by ATM has been shown to promote cellular survival and DNA repair. For example, the DNA end processor PNKP is phosphorylated by ATM at Ser^{114} and Ser^{126}, and this has been shown to be crucial for cellular survival following DSB induction and to enhance PNKP activity (34). Additionally, the phosphorylation of another DNA end processor, tyrosyl-DNA phosphodiesterase (TDP1), by ATM, promotes cellular survival and DNA repair following the induction of DSBs (35). Consistent with these data, the ATM-dependent phosphorylation of APLF at Ser^{116} was found to be important for the cellular survival following IR, efficient DSB repair kinetics, the association of XRCC4 with irradiated chromatin and for

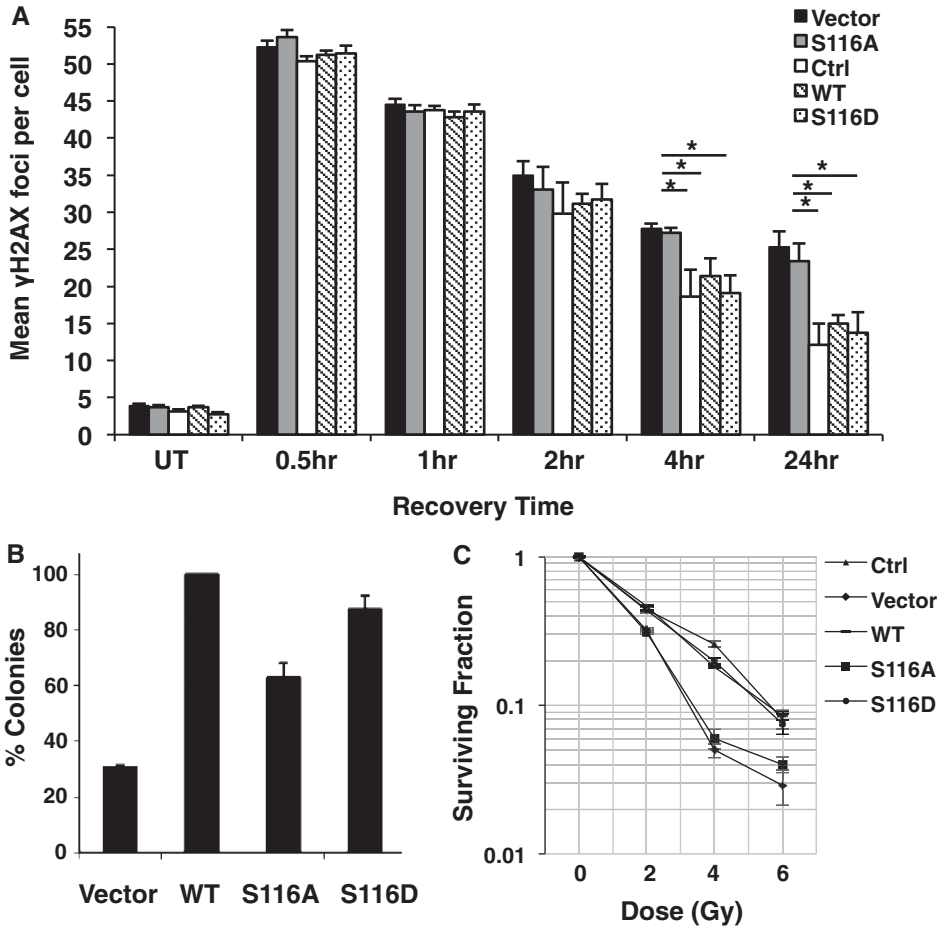

Figure 5. APLF-S116A is associated with defective DSB repair kinetics and increased radiosensitivity. (**A**) U2OS cells stably depleted of APLF by shRNA (U2OS-APLF^{KD}) were reconstituted with empty vector, RNAi-resistant V5-tagged APLF^{WT}, APLF^{S116A} or APLF^{S116D}. G_0/G_1 cells were subjected to 2 Gy γ-IR, and residual γH2AX foci were measured at the indicated recovery periods in cells that were neither positively stained for EdU (S-phase) or undergoing mitosis. The mean number of γH2AX foci per nucleus was quantified for V5 (APLF)-expressing cells. Error bars represent SEM. $*P < 0.01$, using an unpaired student *t*-test. (**B**) U2OS cells expressing empty vector, or RNAi-resistant V5-tagged APLF^{WT}, APLF^{S116A} and APLF^{S116D} were transfected with linearized plasmid DNA, replated at low density in selective media and incubated for 10 days at 37°C. Colonies were stained and quantified 10 days later. Random plasmid integration expressed relative to WT APLF was calculated (% colonies). (**C**) U2OS-APLF^{KD} cells were reconstituted with empty vector, RNAi-resistant V5-tagged APLF^{WT}, APLF^{S116A} or APLF^{S116D} and exposed to 0, 2, 4 or 6 γ-IR. Seven days following damage, colonies were stained with Coomassie Blue dye, and the surviving fraction was calculated. For 5A, 5B and 5C, results are averages from three independent experiments. Mean values ± SEM are indicated. Ctrl; control, U2OS cell line.

APLF-dependent NHEJ (Figure 5, Supplementary Figure S10A and D). Together, our data are consistent with a direct functional link between ATM and APLF-dependent DSB repair.

We have previously shown that the APLF PBZ domains are essential for the initial recruitment of APLF to laser-induced sites of DNA damage, with the first PBZ domain (PBZ1), having the greatest affinity for PAR, being the most critical in this regard (20). Consistent with these data, the affinity of APLF for irradiated chromosomal DNA was also found to be PBZ1-dependent (Figure 4D). In contrast, although the immediate recruitment of the APLF-S116A mutant appeared to be unaffected and similar to WT-APLF (Figure 4A, Supplementary Figure S7A), likely as a consequence of having functional PBZ domains, the single substitution of Ser^{116} to alanine (S116A) resulted in a decreased association with the chromosomal fraction as well as decreased accumulation at the laser tracks after 5 min. Therefore, we wondered what, if any, relationship might exist between APLF-PAR interactions and the ATM-dependent phosphorylation of APLF. Strikingly, the APLF PBZ mutants were compromised in their ability to undergo IR-induced phosphorylation at Ser^{116} (Figure 1F), suggesting that APLF undergoes PBZ-dependent phosphorylation by ATM.

The modulation of early ATM signalling by PAR has been previously described, and PARP1 and ATM have been reported to physically interact (36). Furthermore, PARP1 is strongly activated by DNA damage and plays an important role in facilitating the rapid initial PAR-dependent recruitment of APLF to DNA damage (Figure 3B and C). Therefore, we were surprised that the phosphorylation of APLF at Ser^{116} did not appear to be

influenced by PARP1 depletion and instead was found to be dependent on PARP3. PARP3 interacts with APLF in a PBZ-dependent manner and was found to co-localize with APLF following whole-cell irradiation (Figure 2B and C). These data suggest that APLF undergoes PAR-dependent interactions with PARP3 at DSBs, which is important for its subsequent phosphorylation by ATM. We infer that the PARP1- and PARP2-dependent recruitment of APLF is likely more strongly associated with SSBs, which would not immediately result in ATM activation and would provide an explanation for the lack of defective immediate recruitment of the EGFP-APLF-Ser^{116A} mutant protein.

PARP3 has been shown to be involved in APLF-dependent NHEJ (15), and human cells stably depleted PARP3 (17) or APLF (Figure 5) display similar impairment of DSB repair kinetics. However, little is known about PARP3 with respect to DNA damage signalling. Interestingly, PARP3 and ATM were noted to have very similar effects on APLF DSB damage signalling. The siRNA-mediated depletion or chemical inhibition of either PARP3 or ATM was associated with undetectable IR-induced APLF-Ser^{116} phosphorylation, altered APLF recruitment kinetics and decreased association with irradiated chromatin. ATM inhibition or PARP3 depletion had more modest effects on early APLF recruitment kinetics compared with PARP1 or PARP2 siRNA-mediated depletion, but the chemical inhibition of PARP1/2 with PJ-34 did not impact on the later accumulation of APLF and pSer^{116} detected at the tracks (Supplementary Figure S6). This may be due to the robust activation of PARP1 and PARP2 catalytic activity immediately following DNA damage (37), which would lead to strong PBZ-dependent recruitment of APLF. In contrast, PARP3 has weaker ADP-ribosylation activity (15) and, like ATM-dependent phosphorylation, would be expected to be associated with DSB damage signalling. More specifically, this association with DSB signalling may result in delayed temporal requirements for PARP3 and ATM with regard to APLF recruitment kinetics and the interaction with DNA damage. The involvement of APLF in SSB sensing and signalling might be anticipated to occur earlier, as has been previously suggested (38).

The chemical inhibition of ATM activity also abrogated PARP3 recruitment, suggesting that ATM and PARP3 may participate in a common signalling pathway with APLF. Further evidence for a common pathway was suggested by the lack of an additive effect of combined ATM inhibition with PARP3 depletion on APLF recruitment kinetics in U2OS cells (Figure 4C, Supplementary Figure S8). Therefore, PARP3 appears to be recruited to DNA damage in an ATM-dependent manner. PARP3 likely participates downstream of ATM in this pathway, as ATM activation (as monitored by autophosphorylation at ATM-Ser^{1981}) was not affected by siRNA-mediated PARP3 depletion (Figure 4B). Although some reports in the literature suggest that early ATM signalling may be modulated by PAR (36), other studies have demonstrated that PARP inhibition does not affect ATM activity and in fact might even enhance it (33,39). For example, the prolonged treatment with PARP inhibitors has been shown to lead to an increased burden of endogenous SSBs, which may then be converted into DSBs during replication, thereby resulting in ATM activation (39). Indeed, many studies have shown that continuous PARP inhibition leads to the accumulation of DSBs, which, in DSB repair deficient cells (such as BRCA1/2-deficient cells), are not repaired efficiently and results in increased cell death (40). Therefore, the effects of PARP inhibition on ATM signalling are likely complex and may depend on the specific cellular context.

The other aspect of PARP inhibition to consider is that PARP inhibitors function in essentially the same manner, via competitive inhibition of the PARP substrate, nicotinamide adenine dinucleotide, thereby preventing PAR synthesis (41). As the catalytic domains of PARP1, PARP2 and PARP3 are closely related, PARP inhibitors can target all three DNA damage activated PARPs. Our data, as well as previous reports, suggest that some PARP inhibitors might differ in their relative selectivity for PARP3 (28), as only AZD2281 pre-treatment resulted in impaired IR-induced APLF-Ser^{116} phosphorylation. Therefore, it is possible that the ability of PARP inhibitors to additionally target PARP3 might be important for their clinical use.

Collectively, our data suggest that the ATM-dependent phosphorylation of APLF at Ser^{116} modulates the interaction and the biological function of APLF at DSBs. We propose a model whereby APLF, through its PBZ-domains, is recruited to sites of DSB damage in a PAR-dependent manner, with the kinetics of accumulation of APLF at DSBs being influenced by Ser^{116} phosphorylation. It is possible that APLF undergoes phosphorylation before or following recruitment to sites of DNA damage, but, in the context of DSBs, it appears that the PAR-dependent interaction with PARP3 is important for the subsequent phosphorylation of APLF by ATM. These data suggest that this novel signalling pathway consisting of ATM, PARP3 and APLF enhances the retention of Ser^{116}-phosphorylated APLF at DSBs, which in turn facilitates APLF-dependent NHEJ.

SUPPLEMENTARY DATA

Supplementary Data are available at NAR Online: Supplementary Methods and Supplementary Figures 1–10.

ACKNOWLEDGEMENTS

The authors are grateful to Dan Durocher for his comments and suggestions. They thank the Advanced Optical Microscopy Facility at the Ontario Cancer Institute (University Health Network) for support with live-cell imaging analyses.

FUNDING

Canadian Institutes of Health Research [MOP-102691 to C.A.K.]; the Terry Fox Foundation Strategic Training

Initiative for Excellence in Radiation Research for the 21st Century at Canadian Institute of Health Research, and the Lawrence, Ila and William Gifford Scholarship Fund. Funding for open access charge: Canadian Institutes of Health Research and the Radiation Medicine Program, University Health Network.

Conflict of interest statement. None declared.

REFERENCES

1. Dery,U. and Masson,J.Y. (2007) Twists and turns in the function of DNA damage signaling and repair proteins by post-translational modifications. *DNA Repair*, **6**, 561–577.
2. Vilenchik,M.M. and Knudson,A.G. (2003) Endogenous DNA double-strand breaks: production, fidelity of repair, and induction of cancer. *Proc. Natl Acad. Sci. USA*, **100**, 12871–12876.
3. Shrivastav,M., De Haro,L.P. and Nickoloff,J.A. (2008) Regulation of DNA double-strand break repair pathway choice. *Cell Res.*, **18**, 134–147.
4. Helleday,T., Lo,J., van Gent,D.C. and Engelward,B.P. (2007) DNA double-strand break repair: from mechanistic understanding to cancer treatment. *DNA Repair*, **6**, 923–935.
5. Hakem,R. (2008) DNA-damage repair; the good, the bad, and the ugly. *EMBO J.*, **27**, 589–605.
6. Durocher,D. and Jackson,S.P. (2001) DNA-PK, ATM and ATR as sensors of DNA damage: variations on a theme? *Curr. Opin. Cell Biol.*, **13**, 225–231.
7. Canman,C.E. and Lim,D.S. (1998) The role of ATM in DNA damage responses and cancer. *Oncogene*, **17**, 3301–3308.
8. Chan,D.W., Mody,C.H., Ting,N.S. and Lees-Miller,S.P. (1996) Purification and characterization of the double-stranded DNA-activated protein kinase, DNA-PK, from human placenta. *Biochem. Cell Biol.*, **74**, 67–73.
9. Zolner,A.E., Abdou,I., Ye,R., Mani,R.S., Fanta,M., Yu,Y., Douglas,P., Tahbaz,N., Fang,S., Dobbs,T. *et al.* (2011) Phosphorylation of polynucleotide kinase/ phosphatase by DNA-dependent protein kinase and ataxia-telangiectasia mutated regulates its association with sites of DNA damage. *Nucleic Acids Res.*, **39**, 9224–9237.
10. Urquhart,A.J., Gatei,M., Richard,D.J. and Khanna,K.K. (2011) ATM mediated phosphorylation of CHD4 contributes to genome maintenance. *Genome Integr.*, **2**, 1.
11. Woodhouse,B.C., Dianova,I.I., Parsons,J.L. and Dianov,G.L. (2008) Poly(ADP-ribose) polymerase-1 modulates DNA repair capacity and prevents formation of DNA double strand breaks. *DNA Repair*, **7**, 932–940.
12. Lindahl,T., Satoh,M.S., Poirier,G.G. and Klungland,A. (1995) Post-translational modification of poly(ADP-ribose) polymerase induced by DNA strand breaks. *Trends Biochem. Sci.*, **20**, 405–411.
13. Yelamos,J., Farres,J., Llacuna,L., Ampurdanes,C. and Martin-Caballero,J. (2011) PARP-1 and PARP-2: New players in tumour development. *Am. J. Cancer Res.*, **1**, 328–346.
14. Schreiber,V., Dantzer,F., Ame,J.C. and de Murcia,G. (2006) Poly(ADP-ribose): novel functions for an old molecule. *Nat. Rev. Mol. Cell Biol.*, **7**, 517–528.
15. Rulten,S.L., Fisher,A.E., Robert,I., Zuma,M.C., Rouleau,M., Ju,L., Poirier,G., Reina-San-Martin,B. and Caldecott,K.W. (2011) PARP-3 and APLF function together to accelerate nonhomologous end-joining. *Mol. Cell*, **41**, 33–45.
16. Rouleau,M., McDonald,D., Gagne,P., Ouellet,M.E., Droit,A., Hunter,J.M., Dutertre,S., Prigent,C., Hendzel,M.J. and Poirier,G.G. (2007) PARP-3 associates with polycomb group bodies and with components of the DNA damage repair machinery. *J. Cell. Biochem.*, **100**, 385–401.
17. Boehler,C., Gauthier,L.R., Mortusewicz,O., Biard,D.S., Saliou,J.M., Bresson,A., Sanglier-Cianferani,S., Smith,S., Schreiber,V., Boussin,F. *et al.* (2011) Poly(ADP-ribose) polymerase 3 (PARP3), a newcomer in cellular response to DNA damage and mitotic progression. *Proc. Natl Acad. Sci. USA*, **108**, 2783–2788.
18. Macrae,C.J., McCulloch,R.D., Ylanko,J., Durocher,D. and Koch,C.A. (2008) APLF (C2orf13) facilitates nonhomologous end-joining and undergoes ATM-dependent hyperphosphorylation following ionizing radiation. *DNA Repair*, **7**, 292–302.
19. Rulten,S.L., Cortes-Ledesma,F., Guo,L., Iles,N.J. and Caldecott,K.W. (2008) APLF (C2orf13) is a novel component of poly(ADP-ribose) signaling in mammalian cells. *Mol. Cell Biol.*, **28**, 4620–4628.
20. Li,G.Y., McCulloch,R.D., Fenton,A.L., Cheung,M., Meng,L., Ikura,M. and Koch,C.A. (2010) Structure and identification of ADP-ribose recognition motifs of APLF and role in the DNA damage response. *Proc. Natl Acad. Sci. USA*, **107**, 9129–9134.
21. Mehrotra,P.V., Ahel,D., Ryan,D.P., Weston,R., Wiechens,N., Kraehenbuehl,R., Owen-Hughes,T. and Ahel,I. DNA repair factor APLF is a histone chaperone. *Mol. Cell*, **41**, 46–55.
22. Iles,N., Rulten,S., El-Khamisy,S.F. and Caldecott,K.W. (2007) APLF (C2orf13) is a novel human protein involved in the cellular response to chromosomal DNA strand breaks. *Mol. Cell Biol.*, **27**, 3793–3803.
23. Koch,C.A., Agyei,R., Galicia,S., Metalnikov,P., O'Donnell,P., Starostine,A., Weinfeld,M. and Durocher,D. (2004) Xrcc4 physically links DNA end processing by polynucleotide kinase to DNA ligation by DNA ligase IV. *EMBO J.*, **23**, 3874–3885.
24. Franken,N.A., Rodermond,H.M., Stap,J., Haveman,J. and van Bree,C. (2006) Clonogenic assay of cells in vitro. *Nat. Protoc.*, **1**, 2315–2319.
25. Ahnesorg,P., Smith,P. and Jackson,S.P. (2006) XLF interacts with the XRCC4-DNA ligase IV complex to promote DNA nonhomologous end-joining. *Cell*, **124**, 301–313.
26. Bekker-Jensen,S., Fugger,K., Danielsen,J.R., Gromova,I., Sehested,M., Celis,J., Bartek,J., Lukas,J. and Mailand,N. (2007) Human Xip1 (C2orf13) is a novel regulator of cellular responses to DNA strand breaks. *J. Biol. Chem.*, **282**, 19638–19643.
27. Kurz,E.U. and Lees-Miller,S.P. (2004) DNA damage-induced activation of ATM and ATM-dependent signaling pathways. *DNA Repair (Amst.)*, **3**, 889–900.
28. Loseva,O., Jemth,A.S., Bryant,H.E., Schuler,H., Lehtio,L., Karlberg,T. and Helleday,T. (2010) PARP-3 is a mono-ADP-ribosylase that activates PARP-1 in the absence of DNA. *J. Biol. Chem.*, **285**, 8054–8060.
29. Bekker-Jensen,S., Lukas,C., Kitagawa,R., Melander,F., Kastan,M.B., Bartek,J. and Lukas,J. (2006) Spatial organization of the mammalian genome surveillance machinery in response to DNA strand breaks. *J. Cell Biol.*, **173**, 195–206.
30. Kanno,S., Kuzuoka,H., Sasao,S., Hong,Z., Lan,L., Nakajima,S. and Yasui,A. (2007) A novel human AP endonuclease with conserved zinc-finger-like motifs involved in DNA strand break responses. *EMBO J.*, **26**, 2094–2103.
31. Bakkenist,C.J. and Kastan,M.B. (2003) DNA damage activates ATM through intermolecular autophosphorylation and dimer dissociation. *Nature*, **421**, 499–506.
32. Burma,S., Chen,B.P., Murphy,M., Kurimasa,A. and Chen,D.J. (2001) ATM phosphorylates histone H2AX in response to DNA double-strand breaks. *J. Biol. Chem.*, **276**, 42462–42467.
33. Polo,S.E., Kaidi,A., Baskcomb,L., Galanty,Y. and Jackson,S.P. (2010) Regulation of DNA-damage responses and cell-cycle progression by the chromatin remodelling factor CHD4. *EMBO J.*, **29**, 3130–3139.
34. Segal-Raz,H., Mass,G., Baranes-Bachar,K., Lerenthal,Y., Wang,S.Y., Chung,Y.M., Ziv-Lehrman,S., Strom,C.E., Helleday,T., Hu,M.C. *et al.* (2011) ATM-mediated phosphorylation of polynucleotide kinase/phosphatase is required for effective DNA double-strand break repair. *EMBO Rep.*, **12**, 713–719.
35. Das,B.B., Antony,S., Gupta,S., Dexheimer,T.S., Redon,C.E., Garfield,S., Shiloh,Y. and Pommier,Y. (2009) Optimal function of the DNA repair enzyme TDP1 requires its phosphorylation by ATM and/or DNA-PK. *EMBO J.*, **28**, 3667–3680.
36. Haince,J.F., Kozlov,S., Dawson,V.L., Dawson,T.M., Hendzel,M.J., Lavin,M.F. and Poirier,G.G. (2007) Ataxia telangiectasia mutated (ATM) signaling network is modulated by a novel poly(ADP-ribose)-dependent pathway in the early response to DNA-damaging agents. *J. Biol. Chem.*, **282**, 16441–16453.

37. Smith,S. (2001) The world according to PARP. *Trends Biochem. Sci.*, **26**, 174–179.
38. Haince,J.F., McDonald,D., Rodrigue,A., Dery,U., Masson,J.Y., Hendzel,M.J. and Poirier,G.G. (2008) PARP1-dependent kinetics of recruitment of MRE11 and NBS1 proteins to multiple DNA damage sites. *J. Biol. Chem.*, **283**, 1197–1208.
39. Bryant,H.E. and Helleday,T. (2006) Inhibition of poly (ADP-ribose) polymerase activates ATM which is required for subsequent homologous recombination repair. *Nucleic Acids Res.*, **34**, 1685–1691.
40. McCabe,N., Turner,N.C., Lord,C.J., Kluzek,K., Bialkowska,A., Swift,S., Giavara,S., O'Connor,M.J., Tutt,A.N., Zdzienicka,M.Z. *et al.* (2006) Deficiency in the repair of DNA damage by homologous recombination and sensitivity to poly(ADP-ribose) polymerase inhibition. *Cancer Res.*, **66**, 8109–8115.
41. Rouleau,M., Patel,A., Hendzel,M.J., Kaufmann,S.H. and Poirier,G.G. (2010) PARP inhibition: PARP1 and beyond. *Nat. Rev., Cancer*, **10**, 293–301.